

# Sub-mm sized bubbles injected into metallic melts

F. García-Moreno<sup>a,b</sup>, B. Siegel<sup>a</sup>, K. Heim<sup>a,b</sup>, A.J. Meagher<sup>a,b</sup>, J. Banhart<sup>a,b</sup>

<sup>a</sup> Technical University Berlin, Hardenbergstraße 36, 10623 Berlin, Germany

<sup>b</sup> Helmholtz Centre Berlin for Materials and Energy, Hahn-Meitner-Platz 1, 14109 Berlin, Germany

Email: garcia-moreno@helmholtz-berlin.de, Tel. +49 30 806242761, Fax: + 49 30 806243059

Liquid metal foams containing small equally sized bubbles are expected to be stable, with high liquid fractions. We concentrate on foaming processes of Al-alloy melts following the gas injection route and review briefly the theory about bubble formation in a liquid by gas injection. Several strategies of reducing the bubble size are presented. We discuss how the size and geometry of the gas injector, the gas pressure control and the oscillation of the injector influence bubble size. We also combine some of the strategies and demonstrate that it is possible to produce sub-millimetre bubbles in liquid Al-alloy by gas injection. X-ray observation of the process allows us to evaluate in-situ the changes in bubble size during foam formation in the molten state. Through metallographic cross-sections we can corroborate the bubble size distribution once cooled down and solidified. Alignment of bubbles could be observed and, therefore, even ordering could be possible in future as it is the case in aqueous foams. Finally, we compare metal foam with aqueous foams, emphasising similarities and differences, and discuss possible applications of micro cellular metal foams.

## 1 Introduction

Aluminium foams combine good mechanical properties such as high stiffness, high energy absorption or damping capabilities with low density [1]. One well-known method to produce closed-cell metal foam is the injection of gas into a melt [2-5] to which  $\mu\text{m}$ -sized solid particles (e.g. SiC, TiB<sub>2</sub>, Al<sub>2</sub>O<sub>3</sub> or MgAl<sub>2</sub>O<sub>4</sub>) have been added for stabilization [5-12]. These particles can be added directly to the melt or synthesised in-situ by chemical or metallurgical reactions [13-15]. The precise interactions that stabilise particle-reinforced foams are not yet known and subject of current and recent research [6, 16-18]. It is known from studies of single liquid metallic films, that serve as a model for isolated cell walls, that films are more stable the smaller their area is [19]. Obviously, to achieve smaller film areas smaller bubbles are required. Additionally, according to the Young-Laplace law, smaller bubbles possess a higher inner gas pressure and their curvature becomes more spherical. The corresponding foams become wet under the influence of capillary action, as it can be observed in aqueous foams [20]. Films are then strongly curved and the area in which their thickness is close to the critical cell wall thickness (40–100  $\mu\text{m}$ ) [21] is small.

Large pores in metal foam components lead to pronounced statistical scatter of properties, while isolated centimetre-long cavities may even be a source of structure/mechanical failure. The frequent occurrence of such pores is a drawback for commercial breakthrough. Therefore, it is desirable to have a more uniform cell size distribution and smaller cell sizes, preferably in the sub-millimetre range. There is a clear and well-known dependence of the mechanical properties of metal foams from density [1, 22] and theoretical models to describe the relationship [23]. Metal foams with sub-millimetre bubbles are assumed to be superior concerning mechanical properties due to their more spherical structure independently from a higher density, but there is no reliable proof of this until now. It is challenging to vary bubble sizes and foam liquid fraction – corresponding to foam density after solidification – independently, as they are linked to each other [24]. Another argument for small pores is that

even if their size dispersion is the same as for large pores, a given component would contain more pores, which leads to less variance of mechanical properties since the chance of big cavities or structural defects is reduced.

In the present work, we apply different strategies to reduce the diameter of bubbles created by gas injection into a melt and combine several of them to achieve metal foams with sub-millimetre bubbles. We discuss the different mechanisms leading to smaller bubbles.

## 2 Experimental

### 2.1 Material

AlSi9Mg0.6 (in wt.%) + 20 vol.% SiC particle (10  $\mu\text{m}$  mean diameter), also commercially known as F3S20S, was molten and cast into a graphite mold of  $70 \times 15 \times 35 \text{ mm}^3$  size. This geometry facilitated remelting the sample inside an X-ray transparent furnace where gas injection experiments were conducted. To avoid particle settling the melt was held in the liquid state as short as possible and stirred before the experiments to provide a homogeneous particle distribution.

### 2.2 X-ray imaging

To image the gas injection process in liquid melts and to study the influence of parameter changes on bubble size we used an X-ray radioscopy setup composed of a micro-focus X-ray source and a flat panel detector, both from *Hamamatsu*, Japan (Fig. 1a). In this source, electrons are accelerated by a voltage of 100 kV at a current of 100  $\mu\text{A}$  and are focused onto a tungsten target within a spot size down to 5  $\mu\text{m}$ . The emerging conical X-ray beam is transmitted by the X-ray transparent furnace windows made of 2-mm thick BN plates with little absorption, but absorbed partially by the 20-mm thick Al alloy melt. For our experiments, a magnification factor of 1.2, corresponding to a pixel size of 42  $\mu\text{m}$  is used and images are acquired at 1 fps. To allow for a higher imaging rate of 4 fps,  $4 \times 4$  binning of detector pixels was also carried out.

### 2.3 Foaming

Fig. 1b shows a sketch of the gas injection furnace. The foaming chamber comprises two TiN heating plates with embedded carbon heating lines with a total power of 1200 W. They are oriented in parallel to the X-ray direction and covered with BN spray. The two 2-mm thick BN plates are oriented perpendicular to the heating plates and act as X-ray windows and a crucible for both the melt and the foam. Due to the heat insulation applied temperatures above 750  $^{\circ}\text{C}$  can be reached. The heating profile is controlled by a temperature controller *CAL 3300* from *CAL controls*, USA, and the corresponding reference temperature is measured directly at the melt by a thermocouple. A further thermocouple located at one of the heating plates protects the system from overheating. Foam is produced in the foaming chamber by first introducing the thin cannula into the melt from below driven by a stepper motor before conducting gas through this cannula. The motor also allows one to oscillate the cannula in the vertical direction with parameters ranging from 1.5 mm amplitude at 1 Hz up to 0.5 mm amplitude at 20 Hz. Argon (99.999 % purity) was used as a foaming gas. Commercially available stainless steel cannulas with an inner diameter  $d_i = 0.2 \text{ mm}$  and an outer diameter of  $d_o = 0.5 \text{ mm}$  with either epidural, cylindrical or conical shape were used. Additionally, a smaller cannula with a reduced sickle-shaped opening was created by inserting a stainless steel wire of a diameter  $d_o = 0.15 \text{ mm}$  in the cannula. The equivalent area

of the opening corresponds to a circle with  $d_i = 0.066$  mm and, although the opening is not circular, it was possible to reduce bubble size with it, see section 4.6.

The gas overpressure in the injector was adjusted by first reducing it coarsely from 200 bar in the gas cylinder to 2 bar by a manual regulator and then fine-tuning it with a needle valve. The pressure was measured using a pressure sensor *Capacitron DM 21* from Leybold, Germany. Using a flow rate controller *MKS Flow PR-3000* from MKS Instruments, Germany, a gas flow up to max.  $100 \text{ cm}^3/\text{min}$  through the injector could be set. Bubbles produced at the cannula orifice detach after reaching a certain critical volume and ascend to the melt surface due to their buoyancy, where they accumulate and produce a liquid foam layer. By switching off the heater the foam can be solidified and conserved for further analysis.

## 2.4 Characterisation

From the X-ray radioscopic sequences, both the bubble and foam formation can be evaluated qualitatively in a first step. Furthermore, the bubble diameter can be analysed quantitatively by means of image analysis software. This is done best just after bubble formation and detachment at the top of the melt where bubbles form the bottom part of the foam layer. At the top of the cannula the contrast is poor due to a large amount of melt in the line of view. During their quick ascension the images of the bubbles are blurred and not usable.

The determination of the bubble diameter was performed by analysing the X-ray images using the commercial software *Adobe Photoshop CS5 Extended*. Bubbles with diameters less than 3 mm could not be analysed properly in this way because of the lack in spatial resolution, but a size range could be given. By recording the diameter of each bubble the mean bubble size of the foam generated can be calculated, irrespective of later coarsening or coalescence during foam evolution. Metallographic cross sections of solidified samples were performed by vertically cutting and grinding the foamed samples, thus providing an independent view of the solid metal foam structure obtained.

## 3 Theory of bubble formation

Several forces act on the boundary surface of a bubble with radii of curvature  $R_1$  and  $R_2$  in the gas-liquid interface: The atmospheric pressure  $P_0$ , the hydrostatic pressure  $P_h$  and the capillary pressure  $P_\sigma$  have to be taken into account. These pressures have to be in equilibrium with the inner bubble pressure  $P_b$  according to Young-Laplace's law:

$$P_b = \sigma \left( \frac{1}{R_1} + \frac{1}{R_2} \right) + h g \rho_l + P_0, \quad (1)$$

with  $P_h = h g \rho_l$ , where  $\rho_l$  is the density and  $h$  the height of the liquid. For spherical bubbles of equal size, their radii are  $R = R_1 = R_2$  and therefore  $P_\sigma = \sigma (2/R)$ .

In the course of gas injection through an orifice into a liquid the gas pressure increases and the bending radii of the emerging bubbles decrease up to a critical radius, where  $R = d_i/2$ . From this point the gas pressure is reduced and the bubble radius increases up to the detachment point [25, 26]. A scheme of pressure course during continuous injection of gas in a melt is shown in [27]. The critical radius corresponds to the maximal pressure inside the bubble  $P_{b,max}$ :

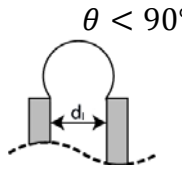
$$P_{b,max} = \sigma \left( \frac{4}{d_i} \right) + h g \rho_l + P_0. \quad (2)$$

To overcome this maximal pressure in the bubble and to allow the bubble to further grow and detach from the orifice, we need to apply at least an overpressure  $P_{over,min}$  of:

$$P_{over,min} = P_{b,max} - P_0. \quad (3)$$

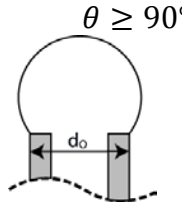
For the special case of producing a bubble with a cannula with an inner and outer diameter, the wettability of the liquid with the material of the cannula plays an important role. For the case that the contact angle  $\theta < 90^\circ$ , the bubble will be formed inside the inner diameter of the cannula while for  $\theta \geq 90^\circ$  at the outer border. The corresponding bubble diameter  $d_b$  is described in Eqs. (4) and (5) [28, 29]:

$\theta < 90^\circ$



$$d_{b,d_i} = \sqrt[3]{\frac{6d_i\sigma}{g(\rho_l - \rho_g)}}, \quad (4)$$

$\theta \geq 90^\circ$



$$d_{b,d_o} = \sqrt[3]{\frac{6d_o\sigma}{g(\rho_l - \rho_g)}}, \quad (5)$$

with the gas density  $\rho_g$ . Therefore cannulas from a material with good wettability in the corresponding liquid, i.e.  $\theta < 90^\circ$ , should lead to smaller bubbles.

However, Eqs. (1–5) are valid for equilibrium conditions only. For real systems with continuous bubble production, especially at higher flow rates, adherence force, dynamic effects and liquid flow considerations have to be taken into account as well as formation of doublets, pairs or turbulent flow and a corresponding reduction of the effective bubble formation pressure in the wake of the previous bubble [26, 30].

## 4 Results

Several production parameters such as the cannula size and geometry, the gas pressure and flow and the oscillation frequency and amplitude of the injector were varied during the production of AlSi9Mg0.6 (in wt.%) + 20 vol.% SiC foams at 700 °C. The corresponding dependencies of the bubble diameter were analysed. Furthermore, some of the measures inducing bubble size reduction were combined to obtain aluminium foam with sub-millimetre sized bubbles. Even smaller cannula diameters than used in this work should lead to even smaller bubbles as it is known from the literature [29], but due to the availability of cannulas we had to restrict the study to the given diameters. In the following we will report on the dependence of the bubble diameter on different parameters.

#### 4.1 Cannula shape

Gas injection experiments with cannulas with the same inner and outer diameters ( $d_i = 0.25$  mm and  $d_o = 0.5$  mm) but different shapes (epidural, cylindrical and conical) were performed at 187 mbar overpressure. Figure 2 shows that the cannula with the epidural shape produces the largest bubbles ( $d_b = 9.8 \pm 0.7$  mm) followed by the cylindrical one ( $d_b = 6.0 \pm 0.5$  mm). With the conical cannula the smallest bubbles ( $d_b = 4.8 \pm 0.4$  mm) could be achieved.

#### 4.2 Gas overpressure

As explained in section 3 a minimal overpressure is needed to form a bubble in a liquid, depending also on the cannula diameter. Figure 3 shows the dependence of the bubble diameter on the gas overpressure in the conical cannula. Although there is a large scatter of values a reduction of the bubble size seems to exist between 147 mbar and 187 mbar, followed by a more or less constant value up to 287 mbar. The opposite trend is observed for the bubble formation frequency, which increases from 0.75 Hz at 147 mbar overpressure up to 2.85 Hz at 287 mbar.

#### 4.3 Gas flow rate

The gas flow rate of the injector was controlled and varied from 20 to 100 cm<sup>3</sup>/min. The dependence of the bubble diameter on the gas flow rate at 187 mbar overpressure for a conical cannula is depicted in Figure 4. An approximately linear decrease in mean bubble size from  $d_b \approx 7$  mm to  $d_b \approx 5$  mm with increasing flow rate is observed, represented by a linear fit. The bubble generation frequency as a function of mean bubble size can be represented by cubic power law. The dispersity of bubble size is larger for high flow rates.

#### 4.4 Oscillation frequency of the cannula

In Figure 5a we can observe a radiography recorded in-situ during the foaming process with a conical cannula and in Figure 5b the corresponding cross-section of the solidified foam. The foam was first processed without oscillating the injector, after which the cannula was oscillated at a frequency of 20 Hz and an amplitude of 0.5 mm. The white dashed line separates the (top) part of the foam produced without oscillations from the (bottom) part foamed with oscillations. This shows that the oscillations reduced the bubble size of the foam by 37.5 % from  $d_b(0 \text{ Hz}) = 4.8 \pm 0.4$  mm to  $d_b(20 \text{ Hz}) = 3 \pm 0.2$  mm.

Furthermore, alignments of bubbles are visible in the bottom part during foam production as well as after solidification as indicated by red dashed lines in Fig. 5b. The angle of the bubble alignments changes from the angle during processing to the angle after solidification.

#### 4.5 Oscillation amplitude of the cannula

As the amplitude of oscillation of the cannula depends on the oscillation frequency and is limited by the motor, a systematic study of the amplitude was performed at only 1 Hz to achieve a wider range for the amplitude. Figure 6 indicates an almost linear decay of the bubble size in the range studied with a decrease of bubble size of 41.5 % applying an amplitude of 1.5 mm compared to the static case.

#### 4.6 Sub-millimetre bubble generation and foam formation

It seems likely that a combination of various individual measures that have been shown to reduce the bubble size could lead further towards the main goal of this paper, the production of sub-millimetre bubbles in liquid Al-alloy and in the corresponding solidified foam. The

following parameters were combined: The smallest possible tip opening (sickle-shaped equivalent  $d_i = 0.066$  mm), oscillations at 20 Hz and 0.5 mm amplitude, a flow rate of 100 cm<sup>3</sup>/min and an overpressure of 187 mbar. The result is seen in Fig. 7. The larger bubbles at the top of the foam were created before oscillation started and the larger bubbles on the bottom are due to the failure of the cannula. However, the bubble in the centre of the sample have a diameter of 0.5–1.0 mm and were created when the oscillation was on and the cannula not damaged. No detailed bubble size distribution analysis could be done in this case, as the resolution of the X-ray images was not high enough for these small bubbles, but the solidified cross-sections corroborates this result.

## 5. Discussion

In this section, we discuss the different dependencies found for the bubble diameter including oscillation of the injector cannula as an effective way of bubble size reduction. Although the theoretical estimations are based on static considerations, dynamic aspects will also be considered. Comparisons with aqueous systems will also be discussed, although the volume of bubbles formed in water is more than one order of magnitude smaller, i.e. the diameter is a factor of around 3 smaller than in liquid aluminium [29]. This has been mainly attributed to the significant difference in surface forces between aqueous and metallic systems and the gas flow rates applied for bubble formation [29].

Bubble size distributions measured by X-ray radioscopy is not the best analysis method due to difficulties in identifying bubbles. Still, this method was preferred, as the only alternative – post-solidification metallographic cross-sections or tomography – can only investigate the system after foam solidification without considering foam evolution, i.e. bubble coarsening, coalescence, collapse, shrinking, etc.

### 5.1 Cannula dimensions, shape and material

According to the theory, see Eqs. (4) and (5) and to numerous experiments with aqueous [31, 32] and metallic foams [28, 29, 33] it is not surprising that the bubble size diameter is directly correlated with the cannula diameter, inner or outer, depending on the wettability of the cannula material by the liquid. Steel is supposed to be wetted easily by liquid Al [29] and should lead to small bubbles generated at the inner cannula diameter, but in our experiments bubble formation was at the outer diameter as observed by X-ray radioscopy. This phenomenon has been found in the literature too and was explained by the oxidation of the steel surface that will change the surface tension and the wetting angle [34]. Moreover, in the presence of residual oxygen, bubbles become more stable by building oxide necks between bubble and cannula, thus hindering and retarding detachment, which leads to further inflation of the bubble and long oxidation times [35].

In some experiments bubble grow beyond the edge of the cannula and detached from the outer surface of the cannula as can be observed in Fig 2, implying that although we used a steel cannula, oxidation of the surface will not allow the cannula to be wetted by the melt properly. With the conical cannula the smallest bubbles could be produced. This result corroborates that the cylindrical cannula is not wetted properly by the liquid and the bubble detaches from the outer diameter, which is smaller for the conical cannula. Accordingly, a larger outer surface is provided by the cylindrically shaped cannula, yielding larger bubbles. The highest outer surface exists for the epidural shape, generating the largest bubbles.

## 5.2 Gas pressure and flow

According to Eqs. (2) and (3) the maximum pressure in the bubble can be estimated as  $P_{b,max} = 182.5$  mbar, with  $d_i = 0.2$  mm,  $h = 50$  mm,  $\rho_l = 2392$  kg/m<sup>3</sup> [36],  $d_i = 0.2$  mm,  $\sigma = 0.854$  Nm [37] and  $g = 9.81$  m/s<sup>2</sup>. This maximum pressure corresponds to the critical pressure we need to succeed with bubble formation. However, we were able to reduce the pressure during bubbling to below 150 mbar at a low bubbling rate below 1 Hz, see Fig. 3. The reason for this may be the slowly starting wake formation, dynamic effects and variations of the atmospheric pressure. Although we can observe a slight decrease of bubble size with pressure in Fig. 3 no clear relation emerges.

In the flow rate range studied, bubble diameter decreases with increasing flow rate unlike from what is known for aqueous foams [38], where very high flow rates ( $> 1$  cm<sup>3</sup>/s) are usually applied, giving rise to large bubbles, double bubble formations and turbulent flow. At lower flows the wake effect may be responsible for an effectively quicker detachment of bubbles, corresponding to a lower gas volume in the bubble and a larger bubble formation frequency. As the bubble diameter decreases linearly with flow rate, the bubble formation frequency follows a cubic power law as shown in Fig. 4, as it is related to the bubble volume.

## 5.3 Cannula oscillation

Oscillating the cannula vertically during gas injection was a challenging experimental task as the melt has to be prevented from flowing from the crucible into the gap of the orifice through which the cannula protruded into the melt, but allow for a motion of the cannula. Once melt flows into the gap and solidifies the cannula is jammed and the experiment fails. Because this problem is stronger for higher oscillation frequencies the maximum frequency was limited to 20 Hz and amplitude to 0.5 mm, giving rise to a bubble reduction of 37.5 % as shown in Fig 5. The effect was similar to that of an increase of amplitude, which was 41.5 %, as shown in Fig. 6. Both effects are linked to each other. For the range of oscillation studied, the amplitude was of the same order, but smaller than the range of the bubble sizes. The bubble size dependence may be different for oscillation amplitudes larger than the bubble size. In the studied range of oscillation, however, the oscillation of the cannula seems to induce an early detachment of the bottom part of the bubble, i.e. its neck. Due to the inertia of the liquid, a sudden retraction of the cannula can lead to a local underpressure and therefore induce closing of the gap between cannula and bubble by the liquid forcing the bubble to detach.

A similar effect of bubble reduction by vibration has been reported by Babcsán et al. in a study concerning the production of sub-millimetre sized bubbles by ultrasonic vibration of either the melt or the injector, but no details about the procedure have been given [39].

Furthermore, bubbles align during foam formation as it is seen in Fig. 5, indicated by red dashed lines. The angle of the bubble alignments seems different during processing (Fig. 5a) and after solidification (Fig. 5b), but the images are not comparable as the first one is an integrated image in X-ray direction during the second one is a cross-section, showing a single plain. Such alignments can be induced by the small size of the bubbles as this has never been reported for larger ones. Also, the stability and a narrow bubble size distribution and the confinement of the crucible walls could play a role.

## 5.4 Sub-millimetre sized bubbles

It was shown in section 4.6 that the generation of sub-millimetre sized bubbles and associated foam formation via gas injection in Al-alloys is possible. Combination of several ways of bubble size reduction according to the bubble size dependences found in this work seems near at hand. However, not all of the parameters can be adjusted independently, e.g. a high

oscillation frequency cannot be combined with a large amplitude of oscillation. Moreover, there are restrictions such as for the use of very thin cannulas or very high critical pressures or flow rates. Reactive liquid Al in combination with oscillations and very thin cannulas can make the system vulnerable to failures. Nevertheless, in spite of all these experimental challenges Fig. 7 shows that the production of sub-millimetre bubbles and the corresponding foam is possible. Some further development is required to obtain a set of procedures that allows one to produce such foams routinely and in larger quantities.

Foams with small bubbles seem to be more homogeneous and stable in the liquid state. This can be explained by the higher liquid fraction in foams with smaller bubbles. Liquid dry foams have a polyhedral cells shape while wet foams a more spherical [20]. The corresponding films are flat in dry foams and strongly curved in wet foams. Wet films reduce gas interdiffusion between the bubbles due to their thickness, which in turn reduces coarsening. Monodispersed small bubbles could align similar as shown in Fig. 5 and therefore, even ordering could be possible in future as in aqueous foams [40, 41] and lead to new properties of metal foam components. Isotropic properties will also allow one to customise the design of foamed parts. New application fields such as electrodes for batteries, catalysis, micro foamed pieces are possible applications of microcellular metal foams. This would correspond to the current trend in polymer foam development [42, 43].

## 6. Conclusions

- The bubble size in liquid AlSi9Mg0.6 (in wt.%) + 20 vol.% SiC decreases upon reducing the cannula diameter through which gas is injected, increasing the gas flow rate, and both the oscillation frequency and amplitude of the cannula.
- Sub-millimetre bubbles can be produced, stabilized and collected as foam by combining a small gas injection cannula with oscillations and optimising other parameters.
- Small bubbles with a narrow size distribution tend to align in planes.

## Acknowledgements

Funding by ESA (Projects AO-99-075) is gratefully acknowledged.

## References

- [1] J. Banhart, Manufacture, Characterisation and Application of Cellular Metals and Metal Foams, *Prog. Mater. Sci.* 46 (2001) 559-632.
- [2] D. Leitlmeier, H.P. Degischer, H.J. Flankl, Development of a Foaming Process for Particulate Reinforced Aluminum Melts, *Adv. Eng. Mater.* 4 (2002) 735-740.
- [3] J. Banhart, Manufacturing Routes for Metallic Foams, *JOM* 52 (2000) 22-27.
- [4] N. Babcsán, D. Leitlmeier, J. Banhart, Metal foams - high temperature colloids: Part I. Ex situ analysis of metal foams, *Colloids Surf. A* 261 (2005) 123-130.
- [5] W. Deqing, S. Ziyuan, Effect of ceramic particles on cell size and wall thickness of aluminum foam, *Mater. Sci. Eng. A* 361 (2003) 45-49.
- [6] T. Wübben, S. Odenbach, Stabilisation of liquid metallic foams by solid particles, *Colloids Surf. A* 266 (2005) 207-213.
- [7] V. Gergely, B. Clyne, The FORMGRIP process: Foaming of reinforced metals by gas release in precursors, *Adv. Eng. Mater.* 2 (2000) 175-178.

- [8] S.W. Ip, Y. Wang, J.M. Toguri, Aluminum foam stabilization by solid particles, *Can. Metall. Q.* 38 (1999) 81-92.
- [9] N. Babcsán, D. Leitlmeier, H.P. Degischer, Foamability of Particle Reinforced Aluminum Melt, *Materialwissenschaft und Werkstofftechnik*, 34 (2003) 22-29.
- [10] N. Babcsán, D. Leitlmeier, H.P. Degischer, J. Banhart, The Role of Oxidation in Blowing Particle-Stabilised Aluminium Foams, *Adv. Eng. Mater.* 6 (2004) 421-428.
- [11] D. Wang, Z.Y. Shi, Effect of Ceramic Particles on Cell Size and Wall Thickness of Aluminum Foam, *Mater. Sci. Eng. A* 361 (2003) 45-49.
- [12] G. Vinod Kumar, M. Chakraborty, F. Garcia-Moreno, J. Banhart, Foamability of MgAl<sub>2</sub>O<sub>4</sub> (Spinel) -Reinforced Aluminum Alloy Composites, *Met. Mat. Trans. A* (2011) 1-11.
- [13] C. Körner, M. Arnold, R.F. Singer, Metal foam stabilization by oxide network particles, *Mater. Sci. Eng. A* 396 (2005) 28-40.
- [14] N.B. K. Kadoi, N. Hideo, Role of Oxide Particles in Aluminum Melt toward Aluminum Foam Fabrication by the Melt Route, *Mater. Sci. Forum* 649 (2010) 358-390.
- [15] G.S. Vinod Kumar, N. Babcsán, B.S. Murty, J. Banhart, Verfahren zur Herstellung von Metallschäumen und Metalschaum, German Patent DE 10 2006 031213.9, 2007.
- [16] J. Banhart, Metal Foams: Production and Stability, *Adv. Eng. Mater.* 8 (2006) 781-794.
- [17] A. Haibel, A. Rack, J. Banhart, Why are metal foams stable?, *Appl. Phys. Lett.* 89 (2006) 154102-154103.
- [18] G. Kaptay, Interfacial Criteria for Stabilization of Liquid Foams by Solid Particles, *Colloids Surf. A* 230 (2003) 67-80.
- [19] K. Heim, G.S.V. Kumar, F. Garcia-Moreno, I. Manke, J. Banhart, Drainage of particle-stabilised aluminium composites through single films and Plateau borders, *Colloids Surf. A* 438 (2013) 85-92.
- [20] D. Weaire, S. Hutzler, *The Physics of Foams*, Oxford University Press, 1999.
- [21] H. Stanzick, M. Wichmann, J. Weise, L. Helfen, T. Baumbach, J. Banhart, Process Control in Aluminum Foam Production Using Real-Time X-ray Radioscopy, *Adv. Eng. Mater.* , 4 (2002) 814-823.
- [22] L. Gibson, M. Ashby, *Cellular solids: structure and properties*, Cambridge Univ Pr, 1999.
- [23] M.F. Ashby, A.G. Evans, N.A. Fleck, L.J. Gibson, J.W. Hutchinson, H.N.G. Wadley, *Metal Foams: A Design Guide*, Butterworth-Heinemann, Boston, 2000.
- [24] C. Körner, F. Berger, M. Arnold, C. Stadelmann, R.F. Singer, Influence of processing conditions on morphology of metal foams produced from metal powder, *Mater. Sci. Technol.* 16 (2000) 781-784.
- [25] P. McGuinness, W. Drenckhan, D. Weaire, The optimal tap: three-dimensional nozzle design, *J. Phys. D: Appl. Phys.* 38 (2005) 3382-3386.
- [26] S.D. Bari, A.J. Robinson, Experimental study of gas injected bubble growth from submerged orifices, *Exp. Therm Fluid Sci.* 44 (2013) 124-137.
- [27] N. Babcsan, *Ceramic Particles Stabilized Aluminum Foams*, PhD thesis, University of Miskolc, Hungary, 2003.
- [28] M. Sano, K. Mori, Bubble Formation from Single Nozzles in Liquid Metals, *Mater. Trans.* 17 (1976) 344-352.
- [29] S.V. Gnyloskurenko, T. Nakamura, Wettability effect on bubble formation at nozzles in liquid aluminum, *Mater. Trans.* 44 (2003) 2298-2302.
- [30] G.A. Irons, R.I.L. Guthrie, Bubble formation at nozzles in pig iron, *Metall. Trans. B* 9(1978) 101-110.
- [31] D. C. Blanchard, L. D. Syzdek, Production of air bubbles of a specified size, *Chem. Eng. Sci.* 32 (1977) 1109-1112.

- [32] H.N. Oguz, A. Prosperetti, Dynamics of bubble growth and detachment from a needle, *J. Fluid Mech.* 257 (1993) 111-145.
- [33] R.J. Andreini, J.S. Foster, R.W. Callen, Characterization of Gas Bubbles Injected into Molten Metals Under Laminar Flow Conditions, *Metall. Trans. B* 8B (1977) 625-631.
- [34] S. Gnyloskurenko, A. Byakova, T. Nakamura, O. Raychenko, Influence of wettability on bubble formation in liquid, *J. Mater. Sci.* 40 (2005) 2437-2441.
- [35] N. Babcsan, F. Garcia-Moreno, D. Leitmeyer, J. Banhart, Liquid-metal foams - Feasible in-situ experiments under low gravity, *Mater. Sci. Forum* 508 (2006) 275-280.
- [36] T. Magnusson, L. Arnberg, Density and solidification shrinkage of hypoeutectic aluminum-silicon alloys, *Metall. Mater. Trans. A* 32 (2001) 2605-2613.
- [37] J. Goicoechea, C. Garcia-Cordovilla, E. Louis, A. Pamies, Surface tension of binary and ternary aluminium alloys of the systems Al-Si-Mg and Al-Zn-Mg, *J. Mater. Sci.* 27 (1992) 5247-5252.
- [38] H. Bai, B. Thomas, Bubble formation during horizontal gas injection into downward-flowing liquid, *Metall. Mater. Trans. B* 32 (2001) 1143-1159.
- [39] N. Babcsan, S. Beke, P. Makk, Method of producing a metal foam by oscillations and thus obtained metal foam product, World Patent WO 2010/064059 A2, 2010.
- [40] A. van der Net, W. Drenckhan, D. Weaire, S. Hutzler, The crystal structure of bubbles in the wet foam limit, *Soft Matter* 2 (2006) 129-134.
- [41] A.J. Meagher, M. Mukherjee, D. Weaire, S. Hutzler, J. Banhart, F. Garcia-Moreno, Analysis of the internal structure of monodisperse liquid foams by X-ray tomography, *Soft Matter* 7 (2011) 9881-9885.
- [42] C. Saiz-Arroyo, J. de Saja, J. Velasco, M. Rodríguez-Pérez, Moulded polypropylene foams produced using chemical or physical blowing agents: structure-properties relationship, *J. Mater. Sci.* 47 (2012) 5680-5692.
- [43] S. Doroudiani, C.B. Park, M.T. Kortschot, Effect of the crystallinity and morphology on the microcellular foam structure of semicrystalline polymers, *Polymer Engineering & Science* 36 (1996) 2645-2662.

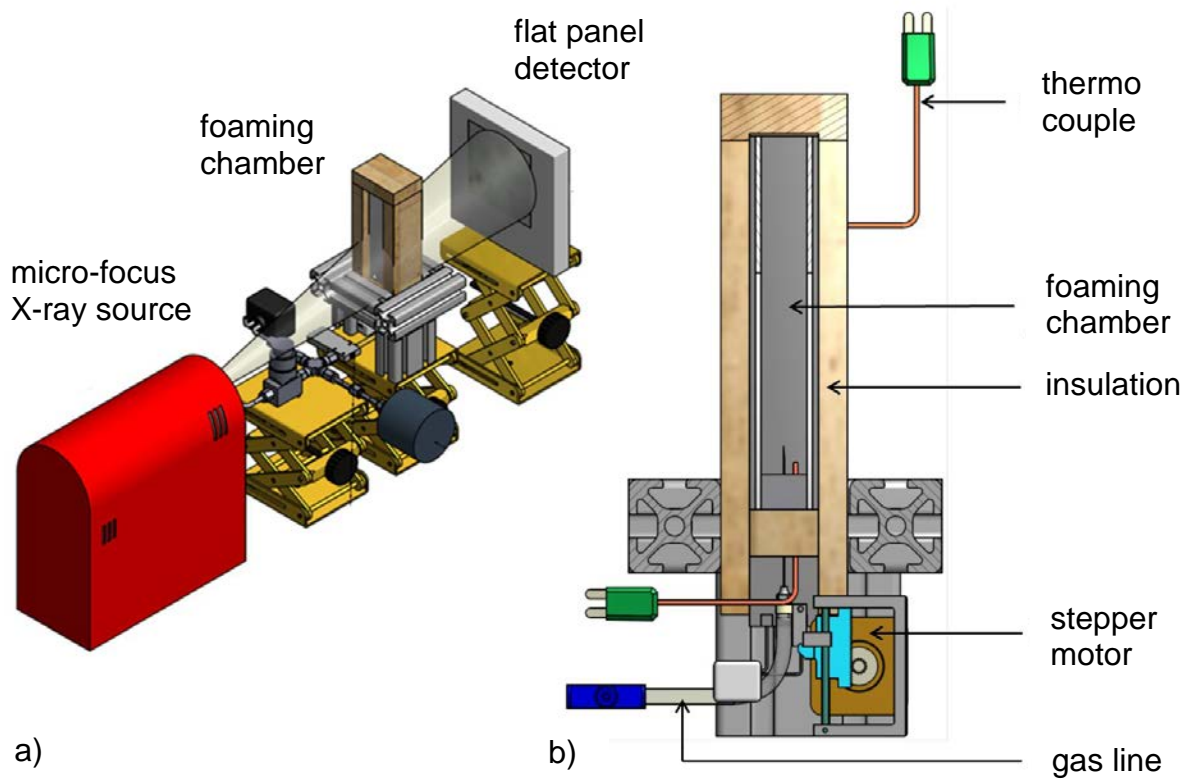


**Figure 1.** a) X-ray radiography setup composed of a micro-focus X-ray source, the foaming chamber and a flat panel detector and b) sketch of the foaming chamber.

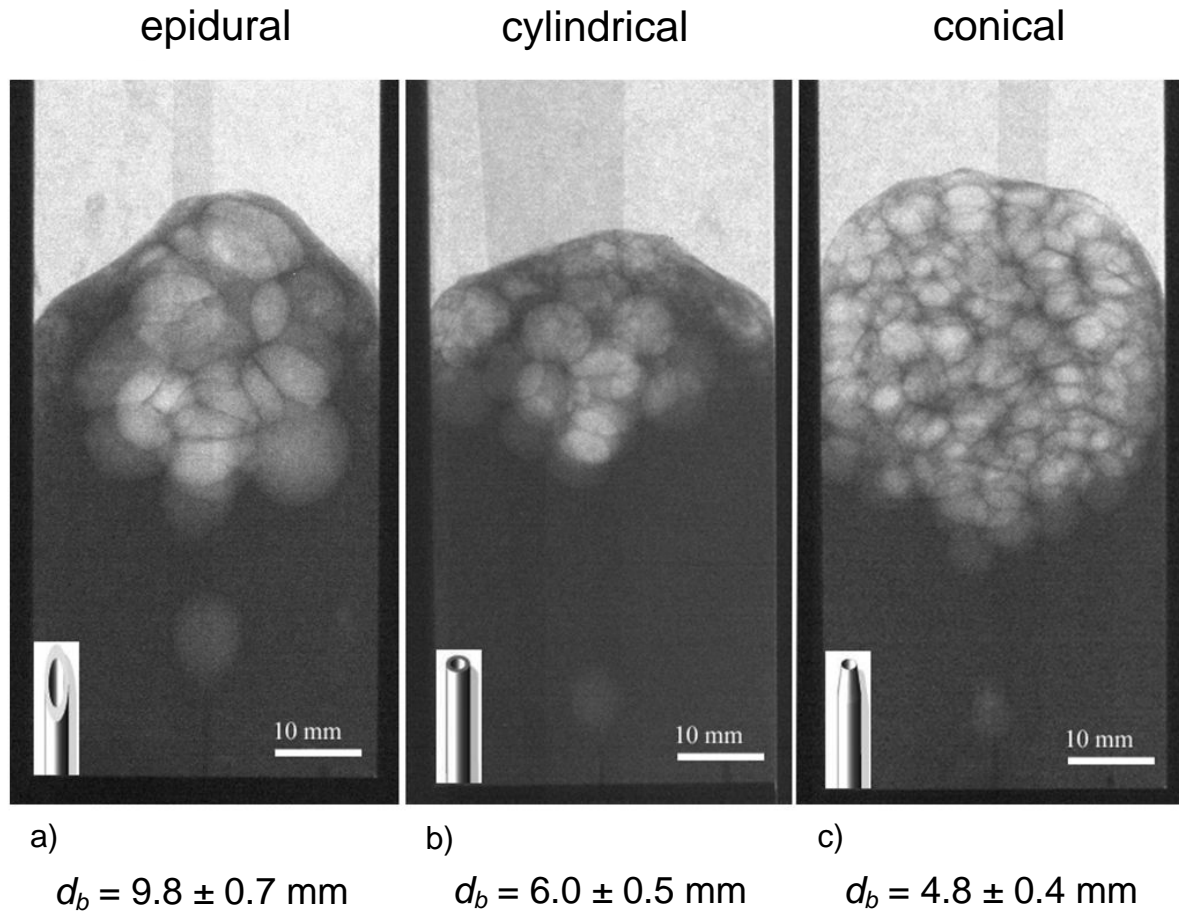


**Figure 2.** Dependence of bubble diameter on cannula shape evaluated for foaming of AlSi9Mg0.6 + 20% SiC at 700 °C and 187 mbar overpressure. a) epidural, b) cylindrical and c) conical.

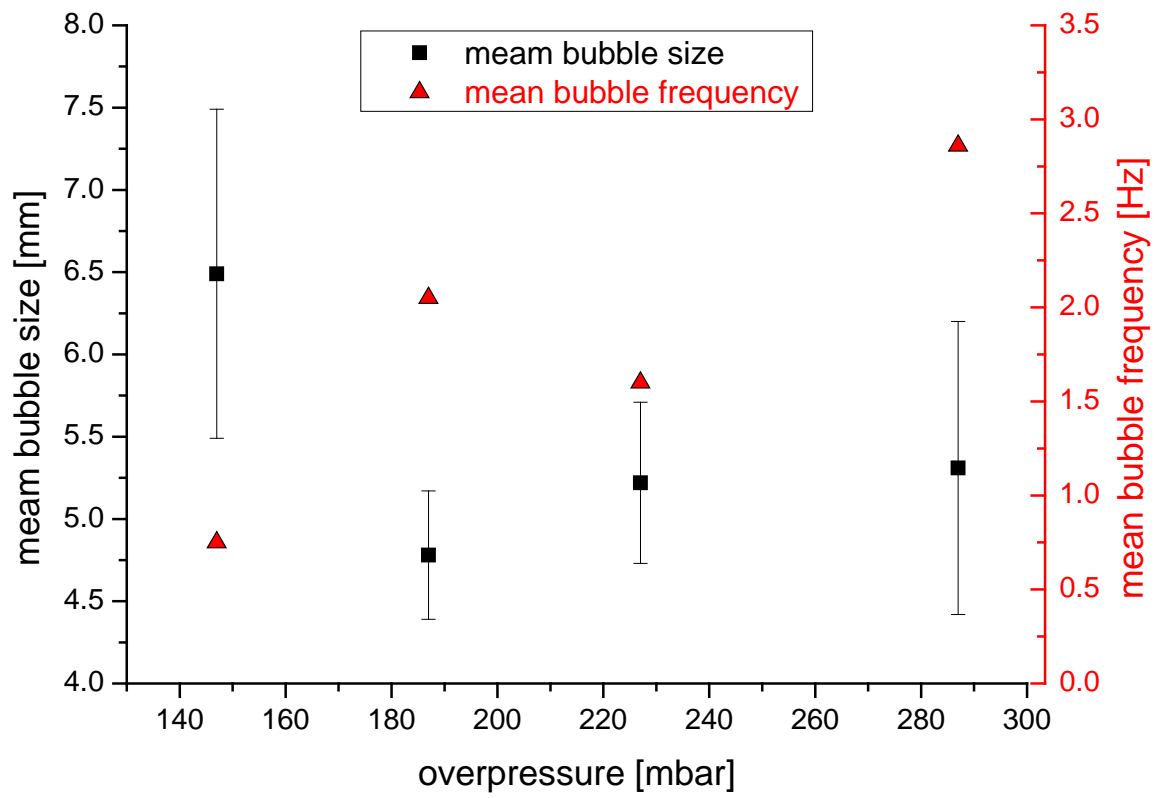


**Figure 3.** Dependence of the bubble diameter on the gas overpressure in the cannula for foaming of AlSi9Mg0.6 + 20% SiC at 700 °C using a conical cannula shape.

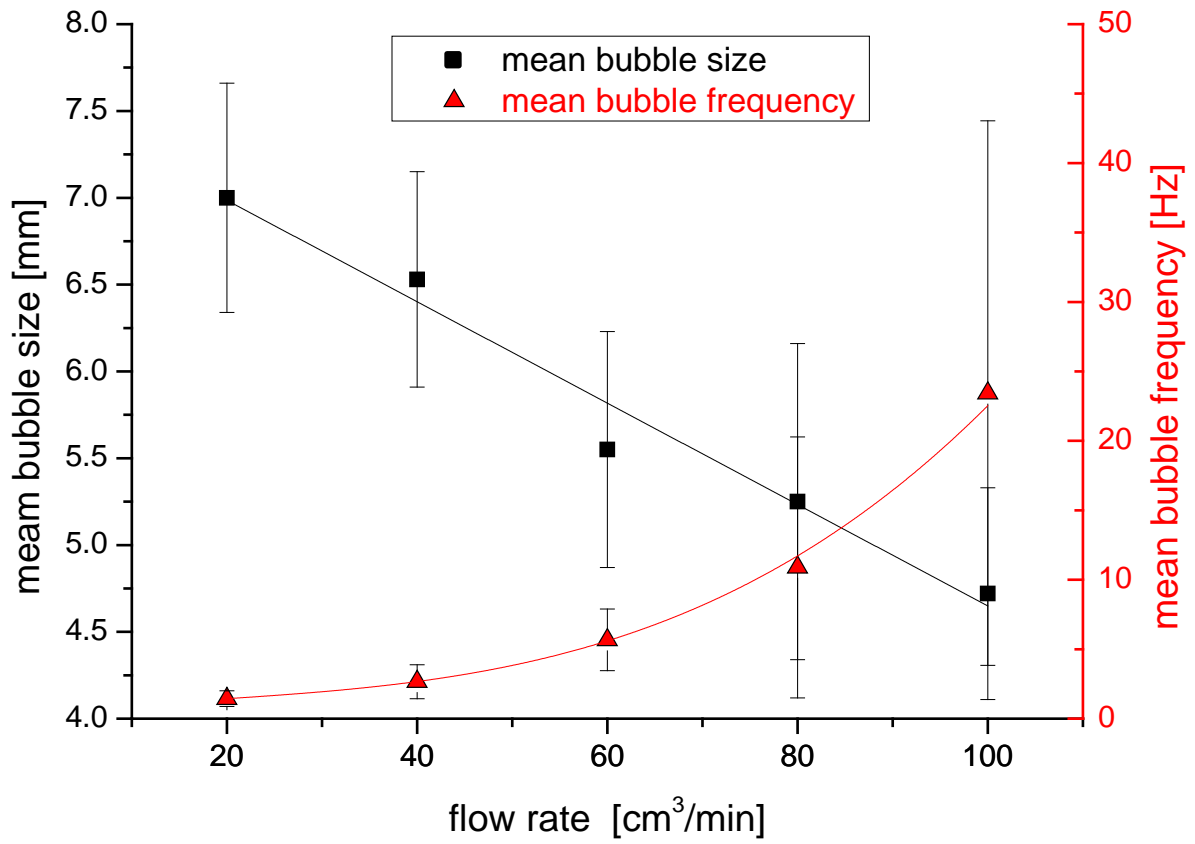


**Figure 4.** Dependence of the bubble diameter on the gas flow rate for foaming of AlSi9Mg0.6 + 20% SiC at 700 °C, 187 mbar overpressure and a conical cannula shape. Black and red lines represent a linear and cubic fit respectively.

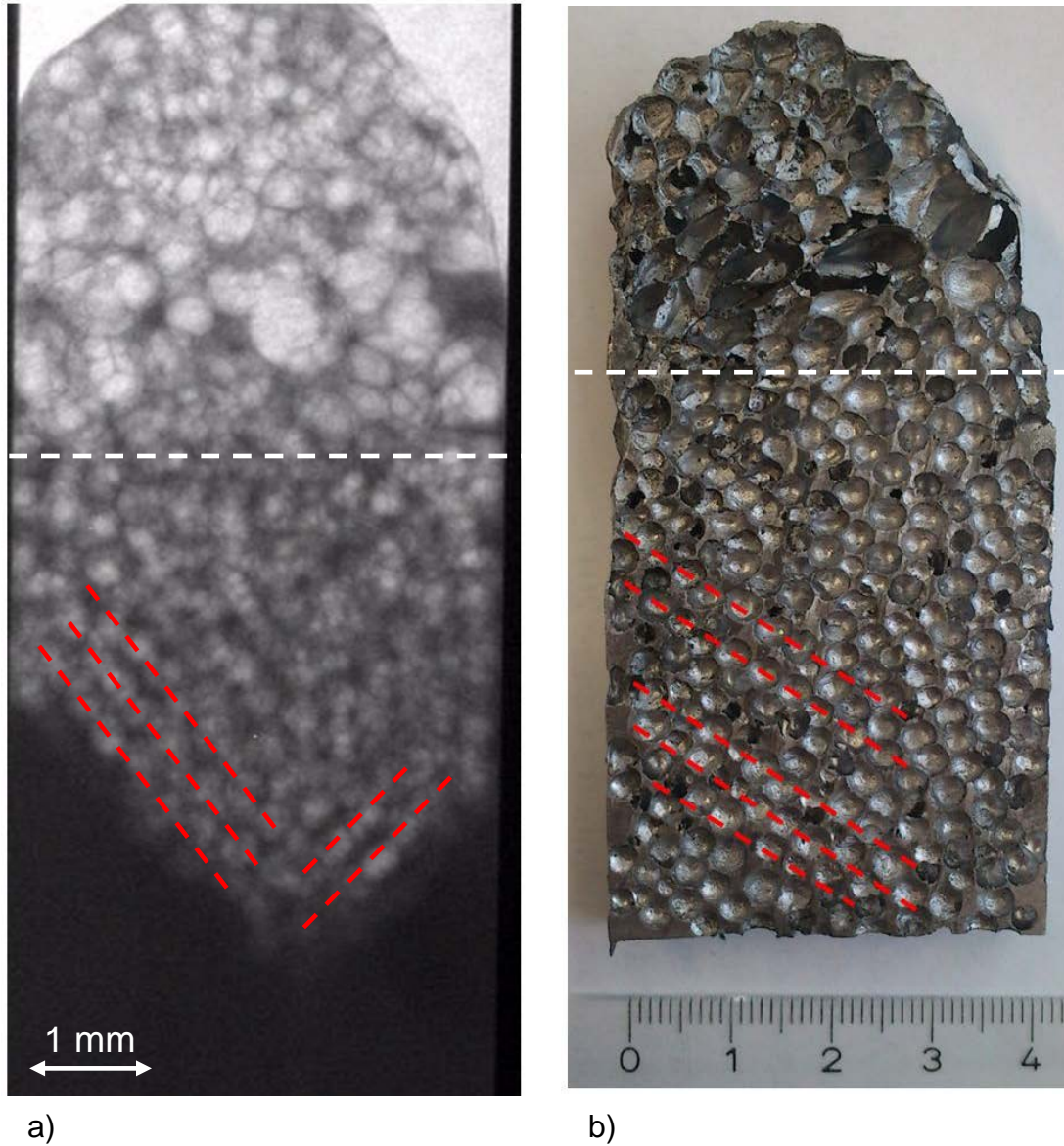


**Figure 5.** a) Radiography acquired in-situ during foaming and b) cross-section after solidification of an  $\text{AlSi9Mg0.6} + 20\% \text{ SiC}$  alloy foamed at  $700\text{ }^\circ\text{C}$  applying a 20 Hz oscillation of a conical cannula. Alignments of bubbles are visible during foam production as well as after solidification as indicated by red dashed lines. The white dashed line delimits the top part foamed without oscillation from the bottom part foamed with oscillation.

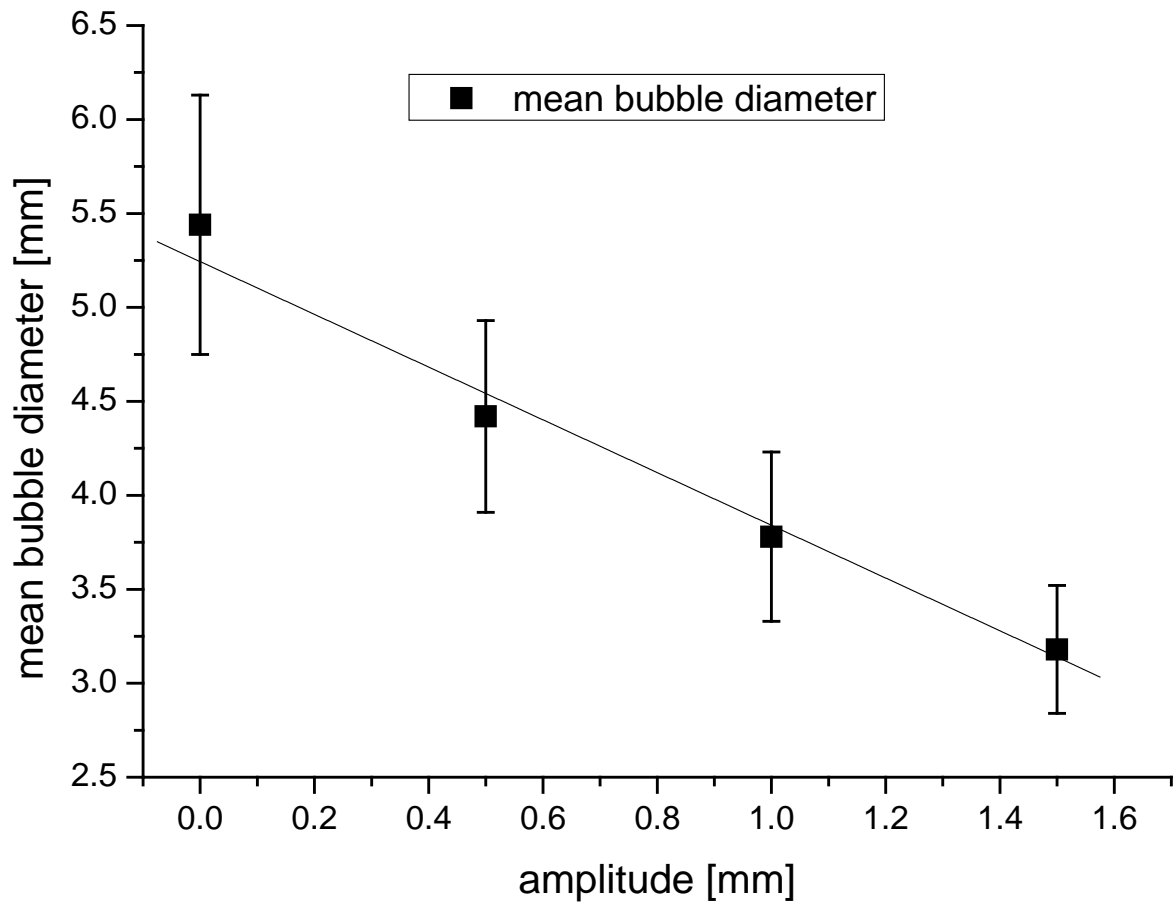


**Figure 6.** Dependence of the bubble diameter on the amplitude of the vibrating cannula at 1 Hz. for foaming of AlSi9Mg0.6 + 20% SiC at 700 °C, 187 mbar overpressure and a conical cannula.

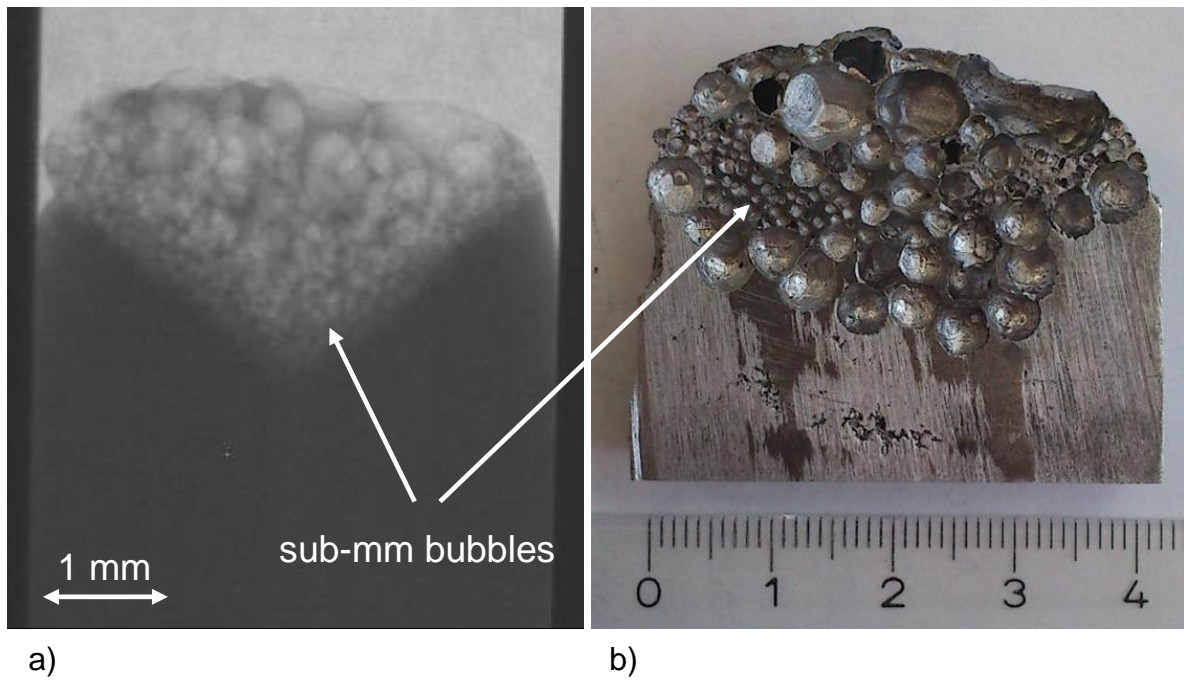


**Figure 7.** a) Radiography taken in-situ during processing and b) cross-section after solidification of an AlSi9Mg0.6 + 20% SiC alloy foamed at 700 °C and 20 Hz oscillation of a conical cannula with 50  $\mu\text{m}$  inner diameter. Very small bubbles in the range of 0.5 to 1 mm diameter are visible during foam production as well as after solidification. If the oscillation stops, bubble diameter increases again.

$d_{i/o}$ [mm]	estimated from Eq. 4 and 5/ experimental condition	$d_b$ . [mm]
0.5	Eq. 5	4.78
0.2	Eq. 4	3.52
0.066	Eq. 4	2.43
$d_i = 0.2$ mm	overpressure:	4.78–6.49
$d_o = 0.5$ mm	187–287 mbar	
$d_i = 0.2$ mm	flow rate:	7.00–4.72
$d_o = 0.5$ mm	20–100 cm <sup>3</sup> /min	
$d_i = 0.2$ mm	oscillation frequency:	4.8–3.0
$d_o = 0.5$ mm	0–20 Hz	
$d_i = 0.2$ mm	oscillation amplitude:	5.44–3.18
$d_o = 0.5$ mm	0–1.5 mm	
$d_i = 0.066$ mm	cannula with wire inside	3–4
$d_i = 0.066$ mm	cannula with wire inside and oscillation: 20 Hz, 0.5 mm	0.5–1.0

**Table 1.** Theoretic bubble size as estimated for bubble generation in AlSi9Mg0.6 + 20% SiC at 700 °C under static conditions according to Eq. 4 and Eq. 5 for different cannula diameter compared with experimental results.